Definition of New Pharmacophores for Nonpeptide Antagonists of Human Urotensin-II. Comparison with the 3D-structure of Human Urotensin-II and URP

Elodie Lescot,[†] Jana Sopkova-de Oliveira Santos,[†] Christophe Dubessy,[‡] Hassan Oulyadi,[§] Aurélien Lesnard,[†] Hubert Vaudry,[‡] Ronan Bureau,*[,†] and Sylvain Rault[†]

Centre d'Etudes et de Recherche sur le Médicament de Normandie, Université de Caen, U.F.R. des Sciences Pharmaceutiques, 5 rue Vaubénard, 14032 Caen Cedex, France, Institut National de la Santé et de la Recherche Médicale (INSERM) U413, Institut Fédératif de Recherches Multidisciplinaires sur les Peptides (IFRMP) 23, Université de Rouen, 76821 Mont-Saint-Aignan, and Institut de Recherche en Chimie Organique Fine (IRCOF), Laboratoire de Resonance Magnetique Nucleaire (RMN), Université de Rouen, 76821 Mont-Saint-Aignan, France

Received September 12, 2006

Starting from nonpeptide agonists and antagonists of human urotensin-II (hU-II), several pharmacophores were designed and compared to the structure of hU-II. NMR and dynamic studies were realized on hU-II and urotensin-II-related peptide to check the conformation flexibilities of these peptides and the relationships between their potential 3D structures and the pharmacophores. In parallel, a virtual screening was carried out, leading to the discovery of six new derivatives with micromolar affinities. This last result shows the interest of these pharmacophores for the discovery of new ligands.

INTRODUCTION

Urotensin-II (U-II) is a cyclic peptide originally isolated from goby fish urophysis.[1] Human urotensin-II (hU-II), subsequently identified and cloned,[2] is the natural ligand of the orphan receptor GPR14,[3] now referred as the UT-II receptor. It was found within vascular and cardiac tissue and appears to be the most potent vasoconstrictor[4−6] known up to now. The peptide is expressed in the central nervous system as well as other tissues such as kidney, spleen, small intestine, colon, placenta, thymus, prostate, pituitary, and adrenal glands.[7−12] hU-II is composed of 11 amino acids (ETPDCFWKYCV),[2] generated by proteolytic cleavage from a precursor prohormone, with a conserved cysteine-linked macrocycle CFWKYC. The sequence WKY appears to be very important for the biological activities,[13,14] whereas the disulfide bridge of hU-II is of minor importance.[7,15] A recent report[11] has demonstrated the existence, in mice, rats, and humans, of a paralog of hU-II (ACFWKYCV for the sequence) named U-II-related peptide (URP), suggesting that the biological effects previously attributed to hU-II could actually be exerted by URP. Structure−activity relationships on URP led to the same conclusion concerning the importance of the sequence WKY toward biological activity.[16]

During the past few years, several nonpeptide U-II antagonists were described in the literature (Charts 1and 2). The most potent correspond to urea derivatives[17−22] such as compounds **1** and **2** with Ki values of 87 and 67 nM, respectively, benzazepine derivatives such as compound **3**[23] (IC_{50} = 1.7 nM), biphenylcarboxamide derivatives[24] such as compound **4** (IC_{50} = 6 nM), and quinoline derivatives[25]

Chart 1

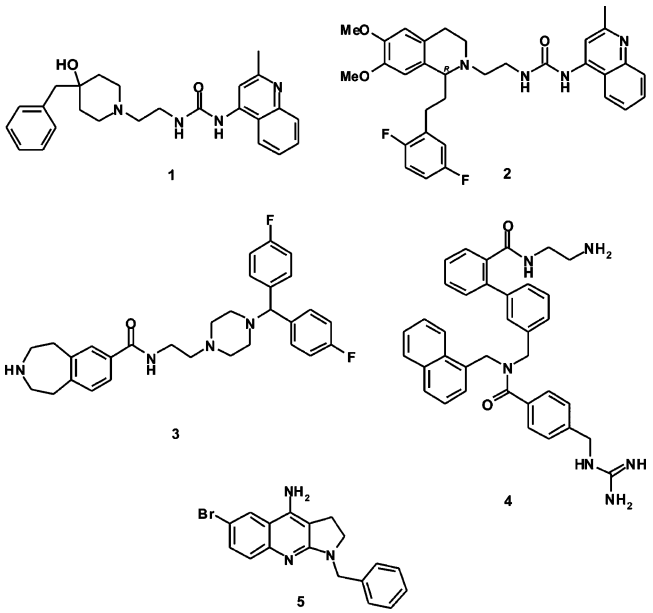

such as compound **5** (IC_{50} = 2.4 nM). Clinical studies of **1** (Palosuran[22]) are currently in progress to examine its effect on diabetic nephropathy. Recently, one publication and several patents (Chart 2) dealt with the preparation of derivatives with lower activities such as compounds **6** and **7**,[26,27] compound **8** such as sulfonamide derivatives,[28−31] and compound **9** such as quinolone derivatives.[32] For these last derivatives, no clear information on the affinity was given (according to the authors, all the compounds described have a submicromolar affinity). Using a pharmacophore model based on the hU-II structure from NMR data, Flohr et al.[13] identified the indole compound **10** (IC_{50} = 0.4 μM) by virtual screening. For the nonpeptide agonist (Chart 3), the screening of a library of 180 000 small organic molecules by Croston

* Corresponding author phone: (33)2-31-43-69-73; fax: (33)2-31-93-11-88; e-mail: ronan.bureau@unicaen.fr.
[†] Université de Caen.
[‡] IFRMP 23, Université de Rouen.
[§] IRCOF, Université de Rouen.

10.1021/ci6003948 CCC: $37.00
Published on Web 01/13/2007

Chart 2

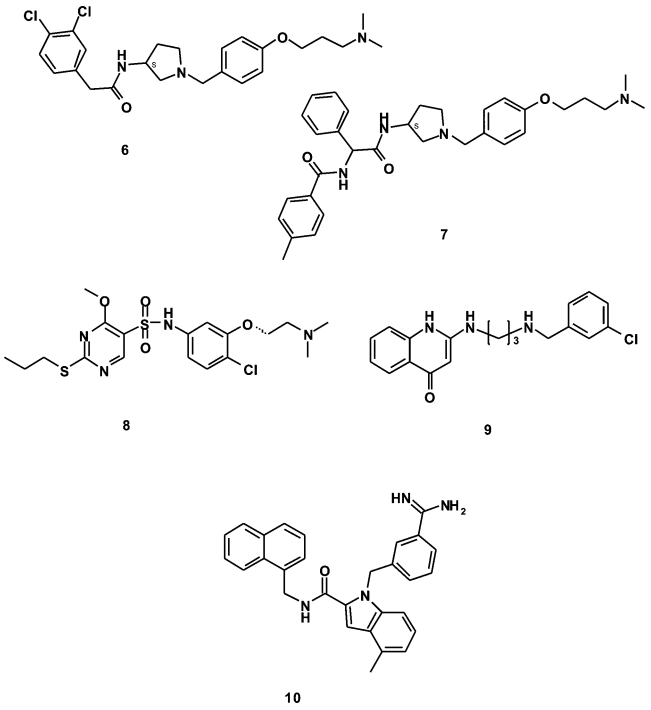

Chart 3

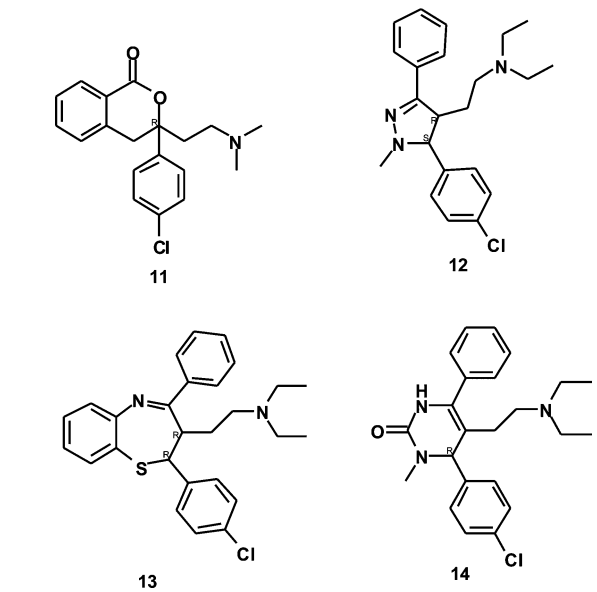

et al.[33] led to the discovery of compound **11** (EC_{50} = 300 nM). Compounds **12**, **13**, and **14** were described in a patent with EC_{50} values of 4, 6.3, and 5 μM, respectively.[34]

Up to now, no pharmacophore has been described for the nonpeptide antagonists of hU-II. For the agonist, only one publication describes pharmacophoric distances associated with peptides and nonpeptides.[35] The present publication focuses on these determinations starting from the most potent ligands. These pharmacophores were compared with the 3D structures (NMR data) of hU-II and URP and also with the conformations resulting from dynamic studies carried out on these peptides. In parallel, the results of the virtual screening of our chemical library are presented.

MATERIALS AND METHODS

Molecular Modeling of Derivatives. The geometry of each compound was built with the Catalyst Software (Catalyst, version 4.9, Accelrys, Inc.) and optimized by using the CHARMm-like force field implemented in the program.[36] Stochastic research coupled to a poling method[37] was applied to generate conformers for each compound of the training set (20 kcal/mol maximum compared to the energy of the most stable conformer).

Definition of the Pharmacophores. The definition of the pharmacophore was based on a common features alignment approach (HipHop method). In this algorithm, the program identifies three-dimensional spatial arrangements of chemical features that are common to all molecules. The model consists of three-dimensional configurations of chemical functions surrounded by tolerance spheres. Principal and MaxOmitFeat values were set to 2 and 0, respectively, to ensure that all of their chemical features would be considered during the definition of the pharmacophore. Misses, feature misses, and complete misses were kept to default values: 1, 1, and 0, respectively. The superposition error, check superposition, tolerance factor, and the weights assigned to each chemical function were set to 1. The minimum interfeature distance was 3 Å.

Virtual Screening. Our chemolibrary (called the CERMN database), containing 6626 compounds resulting from our different research programs in the field of medicinal chemistry, was used. A quasi-exhaustive conformational search was done to generate the conformations for each compound (fast method for Catalyst software). We considered that the poling method[37] for the generation of conformers was not interesting enough to be used for this screening (best method for Catalyst software). Indeed, this last method tries to improve the coverage of the conformational space but with a cost corresponding to a deformation of the potential energy surface. The energy range between the conformers was 20 kcal/mol (maximum value). Using pharmacophores as 3D queries, all the compounds selected must match all the pharmacophoric points.

Calcium Mobilization Assay. CHO cells stably transfected with the UT-II receptor[16] were plated at a density of 5×10^4 cells/well in flat, clear-bottom, black, 96-well plates. After 24 h in the culture, cells were incubated for 1 h in a humidified incubator (37 °C, 5% CO_2) with 2×10^{-6} M fluo-4 acetoxymethyl ester (AM) calcium dye (Molecular Probes, Invitrogen, Cergy-Pontoise, France) in Hank's buffer saline solution (HBSS; Gibco, Invitrogen) buffered with 5×10^{-3} M 4-(2-hydroxyethyl)-1-piperazineethanesulfonic acid (HEPES) and supplemented with 2.5×10^{-3} M probenecid (Sigma-Aldrich, Saint-Quentin Fallavier, France). Cells were washed twice with HBSS/HEPES/probenecid to remove fluo-4 AM from the incubation medium and incubated in 200 μL of the same medium at 37 °C for 20 min. Fluorescence was recorded by using a Flexstation II-96 fluorescence plate reader system (Molecular Devices, St-Grégoire, France) over 3 min with an excitation wavelength of 480 nm and an emission wavelength of 525 nm. After 18 s of recording in basal conditions, 50 μL of test compounds (5-fold final concentration) was added to the incubation medium with the built-in eight-channel pipettor to assess their agonistic activity. To evaluate the antagonistic potency of the test compounds, cells were incubated with each compound over 30 min after fluo-4 AM loading. Then, during fluorescence recording, a pulse of 10^{-7} M hU-II was administered. After subtraction of the mean fluorescence

Table 1. Chemical Shift Value and $^3J_{NH-H\alpha}$ Coupling Constant of Assigned Proton Resonances in the Spectrum of h-UII in a Water Solution at 280 K[a]

	chemical shift (ppm)					
residue	NH	$C^{\alpha}H$	$C^{\beta}H$	$C^{\gamma}H$	other protons	$^3J_{NH-H\alpha}$ (Hz)
Glu1		4.17	1.99	2.36		
Thr2	8.88	4.65	4.17	1.28		7.2
Pro3		4.35	1.88/2.29	2.02	$C^{\delta}H$: 3.73/3.87	
Asp4	8.65	4.51	2.79			6.9
Cys5	8.08	4.57	2.84/3.13			7.9
Phe6	7.96	4.53	2.58/2.90		C2, 6H: 6.97 C4H: 7.20 C3, 5H: 7.21	7.8
Trp7	7.56	4.76	3.03/3.37		2H: 7.22 4H: 7.56 5H: 7.29 6H: 7.21 7H: 7.58 N_1H: 10.35	
Lys8	8.06	3.97	1.53	0.97/1.08	$C^{\delta}H$: 1.56 $C^{\epsilon}H$: 2.88	
Tyr9	7.77	4.62	3.06		C2, 6H: 7.10 C3, 5H: 6.77	7.1
Cys10	8.02	4.69	3.03			7.7
Val11	8.20	4.16	2.18	0.97		7.9

[a] Chemical shift is relative to sodium 2,2-dimethyl-2-silapentane-5-sulfonate (DSS).

background, the baseline was normalized to 100%. Fluorescence peak values were determined for each concentration of the compound, and EC_{50} or IC_{50} values were calculated with the Prism 4.0 software (GraphPad Software, San Diego, CA) using a four-parameter logistic equation to fit peak fluorescence data.

NMR Spectroscopy and Structure Calculation of hU-II. NMR spectra were obtained on a Bruker DMX 600 NMR spectrometer equipped with a triple-resonance probe including shielded z gradients. One- and two-dimensional NMR spectra were obtained at temperatures of 275, 280, 288, 295, and 300 K. NMR samples were prepared by dissolving 4.4 mg of the peptide hU-II in 550 μL of H_2O (10% D_2O) or D_2O. All two-dimensional NMR spectra were recorded in the pure absorption mode by using the method proposed by States et al.[38] The H_2O resonance was suppressed either by a presaturation using continuous irradiation during relaxation delay or by using the gradient pulse WATERGATE.[39] Spin systems identification and sequential assignment were achieved at $T = 280$ K by double-quantum-filtered correlation spectroscopy (DQF-COSY),[40] total correlation spectroscopy (TOCSY),[41] and nuclear Overhauser effect spectrometry (NOESY)[42,43] experiments. The TOCSY spectra were recorded with a spin-lock time of 80 ms by using the MLEV-17 sequence for the isotropic mixing. Five mixing times (150, 200, 250, and 400 ms) were used for NOESY spectra in order to identify diffusion effects. Data were acquired and processed on Silicon Graphics O2 workstation, using XWIN−NMR and Aurelia software (Bruker).

Distance restraints for structure calculation were derived from NOE crosspeaks in the NOESY spectra recorded at 280 K with $\tau_m = 150$ ms, which were converted into distances by volume integration using the Aurelia software (Bruker). The NOE intensity between the geminal Hβ protons, which corresponds to a distance of 1.8 Å, was used for calibration. The consistency of this calibration was

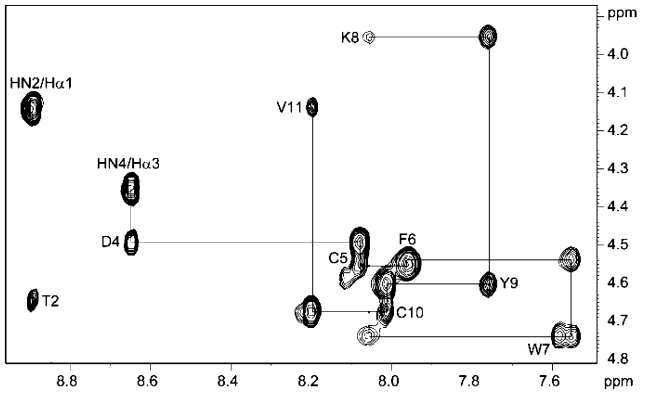

Figure 1. NOESY NH−αCH cross-peaks (dαN) spectrum of hU-II obtained in a water solution at 280 K. The experiment was recorded with a mixing time of 150 ms.

Table 2. Pharmacophore A Toward Nonpeptide Antagonists Considered in the Training Set

compound	activity	fit value	relative energy of conformer[a] (kcal/mol)
2	67 nM	2.15	9.37
3	1.7 nM	2.31	18.15
4	6 nM	3.36	3.04
5	2.4 nM	0.53	0.65

[a] Relative energy of the conformer that fits pharmacophore A, compared to the most stable conformer.

verified on other geminal proton distances. A range of ±25% of the calculated distance was used to define the upper and lower bounds of the restraints. Backbone dihedral restraint residues were deduced from $^3J_{NH-H\alpha}$ coupling constant by using the empirical Karplus-type relations with the Pardi coefficients.[44] For a coupling constant where more than a single Φ value is possible, additional secondary information from NOE data was used to reduce the number of solutions. A range of ±30° was used for defining the upper and lower angles of the constraints.

A total of 69 distance restraints, including short- and long-range inter-residue restraints, and 2 Φ torsion angle restraints were used for structure calculations. The structures were generated from the experimental data with a standard dynamical simulated annealing protocol using the XPLOR_3.1 program.[45]

Dynamic Studies. Molecular dynamics calculations were performed using CHARMm software[36] (Chemistry and HARvard Molecular mechanics) with the potential function parameter set to 27.[46] The peptides were placed in a pre-equilibrated water box (TIP3P[47]) surrounded by identical translated images of itself (PBC conditions). In the hU-II system ($100 \times 77 \times 69$ Å^3 periodic box), the total number of water molecules was 1572 molecules, and in the URP system ($98 \times 77 \times 67$ Å^3 periodic box), the total number of water molecules was 1956 molecules. The model system consisted of all heavy atoms of the proteins and all hydrogens. The potential energy function contains bonded terms representing bond length, valence angle, and torsional (dihedral) angle variations and nonbonded (van der Waals and electrostatic) interactions. The van der Waals interactions were smoothly brought to zero at 14 Å using a shifting function, and the electrostatic interactions were truncated using a switching function acting on a force between 10 and

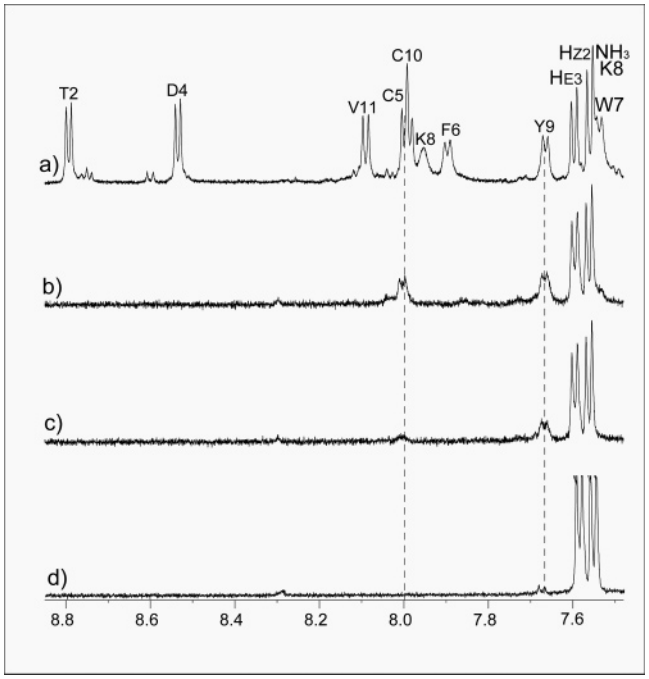

Figure 2. Region of 600 MHz amide proton NMR spectra. (a) Spectrum of hU-II in H_2O. (b−d) Spectra of hU-II in D_2O recorded after 12, 26, and 180 min, respectively.

14 Å. The electrostatic potential energy was calculated using the dielectric constant of vacuum ϵ_o. The system was heated to 300 K in 6 ps in equal increments of 5 K and equilibrated for 50 ps with velocity rescaling. The simulations of 500 ps were carried out for hU-II and URP. Constrain SHAKE was applied to the hydrogens during the dynamic simulation, and a 2 fs time step was used.

Systematic Search. The conformational analysis was carried out with the systematic search module of Sybyl Software (Sybyl Molecular Modeling Package, version 7.0, Tripos, St Louis, MO). The increment was 60° (no modification of the conformational space observed with an increment of 30°) for all rotatable bonds of the lysine residue. The van der Waals radius scale factors were 0.95 (general), 0.87 (interactions 1−4), and 0.65 (possible H bond).

RESULTS AND DISCUSSION

NMR Solution Structure of hU-II. Proton resonances of hU-II in water at 280 K are reported in Table 1. TOCSY and COSY spectra were used to assign spin systems of most of the amino acid residues, and NOESY data provided the sequential connections between these spin systems (Figure 1).

The hU-II secondary structure was deduced from the analysis of the following NMR data: NOE cross-peaks dNN, dαN, and dβN;[48−50] measurement of the 3JNH−Hα coupling constant;[44,51,52] and amide protons' exchange times.[53−57] In the present study, amide protons which were relatively slow to exchange were identified by dissolving hU-II in deuterated solvent D_2O. Then, one-dimensional ^{1}H NMR spectra were recorded at regular intervals (Figure 2). Because of slow H/D exchange, the amide NH of residues Cys10 and Tyr9 disappeared slowly (more than 20 min and 3 h, respectively) compared to the other amide protons.

The dipolar correlations observed in the hU-II NOESY spectrum recorded with a mixing time of 150 ms were

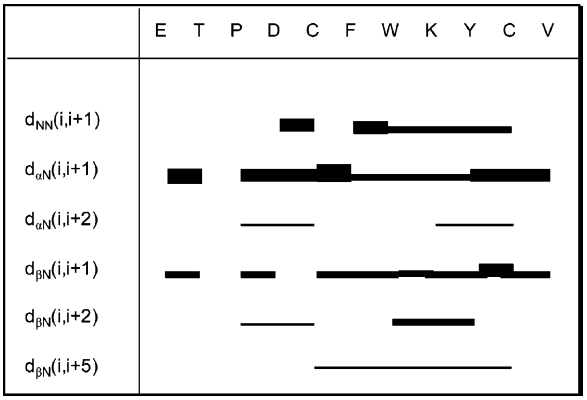

Figure 3. Summary of short and medium NOE observed in a 600 MHz NOESY spectrum (mixing time 150 ms) of hU-II at a temperature of 280 K. The sequence is displayed with a one-letter code. The heights of the bars indicate the intensities of the NOEs.

consistent with a good structuring of this peptide. The observed αi-Ni+1 NOEs, in addition to those present between αi-Ni+2, βi-Ni+2, and βi-Ni+1, are summarized in Figure 3. An examination of short- and medium-range distance restraints reveals the location of the secondary structure in the cyclic region. In particular, NOEs observed between HN-Tyr9 and Hβ-Trp8 as well as HN-Cys10 and Hα-Lys8, in combination with the slow H/D exchange times of NH-Tyr9 and NH-Cys10, suggest a turn centered on Trp7, Lys8, Tyr9, and Cys10.

In order to identify the type of turn and its exact location, molecular modeling calculations under experimental NMR restraints were performed. NOEs obtained in the NOESY spectrum recorded with mixing times of 150 ms and coupling constants measured on the 1D ^{1}H NMR were then used to drive a set of 69 distances and two dihedral angles which were introduced as restraints in molecular dynamics simulation.

A total of 40 structures were generated with a simulated annealing protocol. All the calculated structures fitted the experimental data quite well and converged with high precision. None of the structures displayed violations of the distance restraints larger than 0.03 nm. The absence of long-range NOEs for the N-terminal residues Glu1−Asp4 suggested that the molecule could adopt different tertiary structures. It was therefore not surprising that the resulting structures did not converge to the same global conformation. Figure 4a shows the 20 structures with the lowest energies, fitted to the Cα atoms of residues Cyc5 to Cys10. The residues in this cyclic part were well-defined in terms of Cα position, and the average root-mean-square deviation (RMSD) for the backbone atoms was 0.033 nm. The N-terminal residues showed larger RMSD values for the backbone atoms and wider dispersion of the Φ and Ψ angle values, indicating that these residues are undergoing significant motion on a fast time scale.

Analysis of the calculated structures revealed short distances between the NH of Tyr9 and the carbonyl group of the Trp7 residue (<0.35 nm) and between the NH of the Cys10 residue and the C═O of Lys8 (<0.20 nm). These proximities, as well as the slow-exchange H/D observed for amide NH of the Tyr9 and Cys10 residues, suggest the formation of (i, i + 2) hydrogen bonds. These observations in combination with the (Φ, ψ) dihedral angles of residues

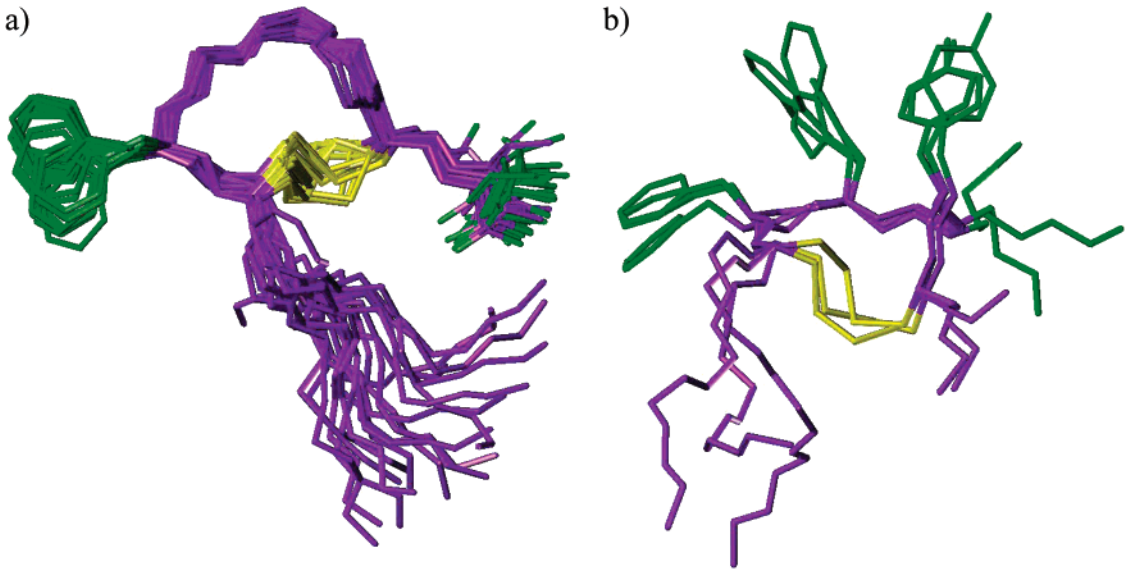

Figure 4. Superimposition of the backbone atoms of refined structures of hU-II. Structures were superimposed by fitting Cα atoms of residues Cys5−Cys10: (a) 20 best structures and (b) three best structures with the side chains of Phe6, Trp7, Lys8, and Tyr9.

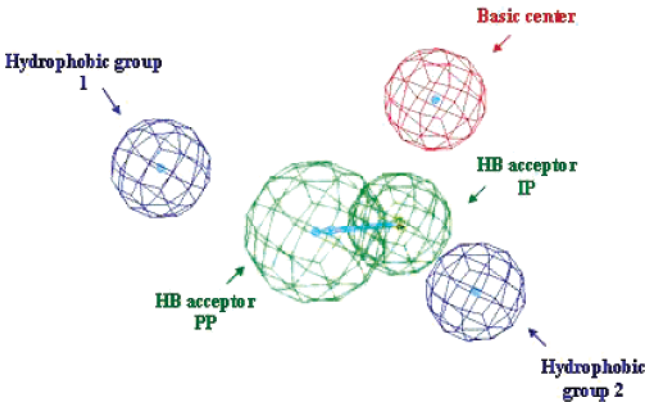

Figure 5. Pharmacophore A.

Tyr9 (−87, 44) and Lys8 (−110, 2) suggested the existence of a distended inverse γ turn centered on Trp7−Lys8−Tyr9 and a standard inverse γ turn centered on Lys8−Tyr9−Cys10.

Although no specific restraints (i.e., $\chi 1$ restraints) were used, the side chains of hydrophobic residues adopted a preferential orientation, and the structure of hU-II showed a hydrophobic face encompassing residues Phe6, Trp7, and Tyr9 (Figure 4b).

Pharmacophore A for the Nonpeptide Antagonists. Four nonpeptide antagonists corresponding to compounds **2**, **3**, **4**, and **5** were chosen according to their biological data and their affinities (Chart 1 and Table 2). In function of their chemical structures, hydrogen-bond acceptor and donor, ionizable group (basic amine), and aromatic hydrophobic features were selected as functional groups. The 10 hypotheses (pharmacophores) generated by the program were all formed by two hydrophobic features, one hydrogen-bond acceptor and one ionizable group; the differences concerned the 3D position of these features. The selected hypothesis, called pharmacophore A (Figures 5 and 6), had the best average fit values (2.08 Å) for all the compounds of the training set (the optimum value is 4). Moreover, we observed for this hypothesis a good relationship between this hypotheses and the previously published pharmacophore based on the structure of hU-II (NMR data).[13] The distances between the chemical features are summarized in Table 3. Compounds **2**, **3**, and **4** fit correctly pharmacophore A with high-energy conformers (Table 2). The particular structural rigidity of **5** led to a lower fit value. The fit value toward this pharmacophore for the other described nonpeptide antagonists shows that compounds **1**, **7**, and **10** fit all the characteristics. The fit values of zero for compounds **6**, **8**, and **9** (Table 4) correspond to a partial fit toward the pharmacophore (at least one feature is missing).

Virtual Screening. The virtual screening of the CERMN database based on pharmacophore A yielded 231 compounds. These derivatives were clustered with the JChem software[58] by a nonhierarchical method, leading to 40 clusters and 75 singletons. The final selection for the initial biological test was based on three criteria: the fit value, the chemical similarities between the families, and the conformations of the fitted compounds. On the basis of these considerations, 17 compounds were evaluated, in a first set, for their agonistic and antagonistic properties using the calcium mobilization assay. Among these compounds, six derivatives inhibit the hU-II-induced calcium signal (antagonist) with IC_{50} values ranging from 1.4 to 6.36 μM (hit rate of 35%). No compound displays agonist activity. Herein, the structures of five compounds corresponding to five clusters are described in Chart 4. No correlation exists between the fit values and the affinity (Table 5). The sixth compound and the members of its family are actually under study and for this reason are not described in this publication.

Pharmacophore B for the Nonpeptide Agonists. By considering the four nonpeptide agonists (Chart 2), the same approach was applied to generate a pharmacophore (called B). This pharmacophore has the same characteristics as pharmacophore A in terms of features (Figures 7 and 8), with however shorter distances between the aromatic groups and a defined spatial orientation for the aromatic groups (Table 6). The maximum fit value is 4.

Pharmacophore A/B toward hU-II. Flohr et al. described a pharmacophore, close to pharmacophore A, based on the NMR data of hU-II in water. Tryptophan and tyrosine

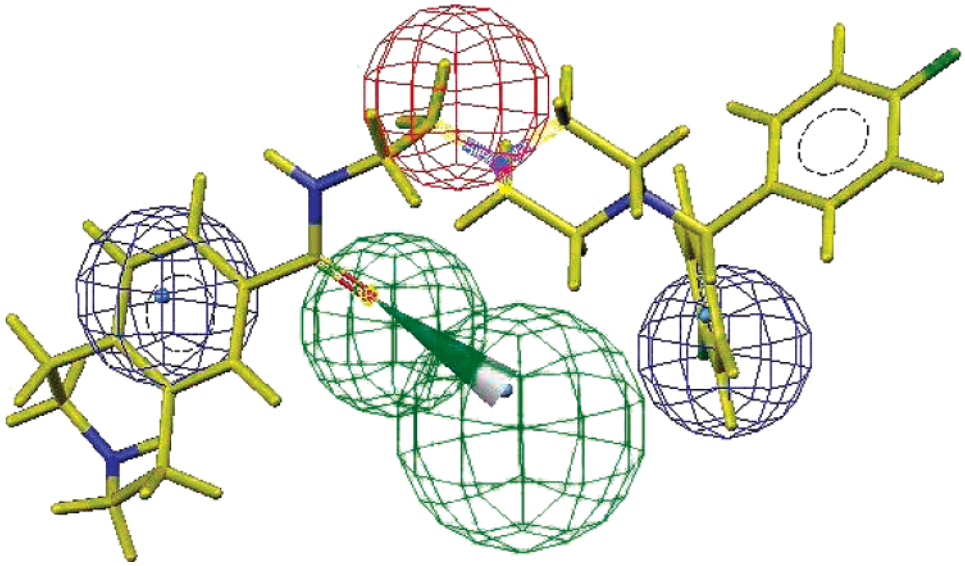

Figure 6. Superimposition between compound **3** and pharmacophore A.

Table 3. Matrix Distances (in Å) for Pharmacophore A[a]

	hydrophobic group 1	hydrophobic group 2	basic center	HB acceptor (PP)
hydrophobic group 1				
hydrophobic group 2	11.43 (*12.2*[b])			
basic center	9.58 (*11.3*[b])	6.81 (*6.4*[b])		
HB acceptor (PP)	8.55	4.47	4.32	
HB acceptor (IP)	6.80	7.02	4.47	3.01

[a] IP: initial point. PP: projected point. [b] Reported distances of hU-II pharmacophore according Flohr et al.[13]

Table 4. Pharmacophore A Toward Various Nonpeptide Antagonists

compounds	activity	fit value	relative energy of the conformer (kcal/mol)
1	87 nM (IC_{50})	3.58	3.53
6	158 nM (IC_{50})	0	N/A
7	390 nM (Ki)	2.03	8.93
8	220 nM (Ki)	0	N/A
9	<1 μM (Ki)	0	N/A
10	400 nM (IC_{50})	2.40	7.25

Table 5. Biological Affinity toward the UT-II Receptor

compound	IC_{50}	fit value	relative energy of the conformer (kcal/mol)
15	2.85 ± 0.52 μM	3.15	11.23
16	2.63 ± 0.32 μM	2.71	17.09
17	6.36 ± 0.32 μM	1.63	9.79
18	1.4 ± 0.25 μM	1.97	16.65
19	3.41 ± 0.73 μM	2.63	11.55
20	3.36 ± 0.18 μM	3.68	7.32

residues were considered for the position of the two hydrophobic features and the lysine residue for the position of the basic center. This pharmacophore is however (vide supra) in contradiction with pharmacophore B, where the distance between the two hydrophobic features is smaller (7.2 vs 12.2 Å). To analyze this first point, in a recent publication[35] on NMR data of hU-II [recorded in a sodium dodecylsulfate (SDS) micelles environment], a distance

Chart 4

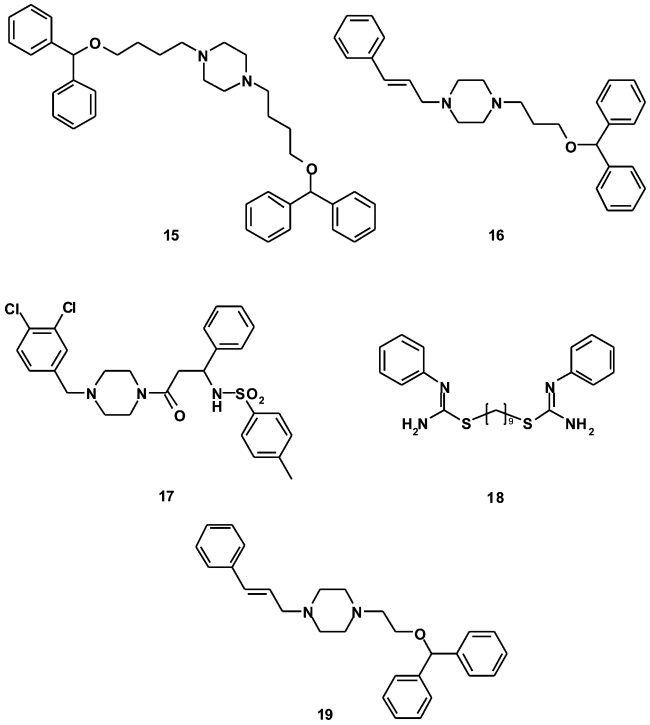

between tryptophan and tyrosine side chains around 5.8 Å was recorded. According to the authors, the different environments (SDS micelles vs aqueous medium for Flohr et al.) can account for the observed discrepancy [5.8 (SDS) vs 12.2 Å (water)].[35] However, the structure of URP[16] or hU-II (vide supra), resolved by NMR in an aqueous environment by our collaborators, led to a distance of approximately 5 Å. So, these last results show a similar Trp7−Lys8 distance whatever the solvent. The second point concerns the relative position of the lysine residue toward the two hydrophobic features and the relationships toward the pharmacophores. On the basis of our NMR data, hU-II and URP show an important variation for the position of the basic group of the lysine residue (Figure 9). To study the conformational flexibility of hU-II and URP and particularly the variations in side-chain positions of the funda-

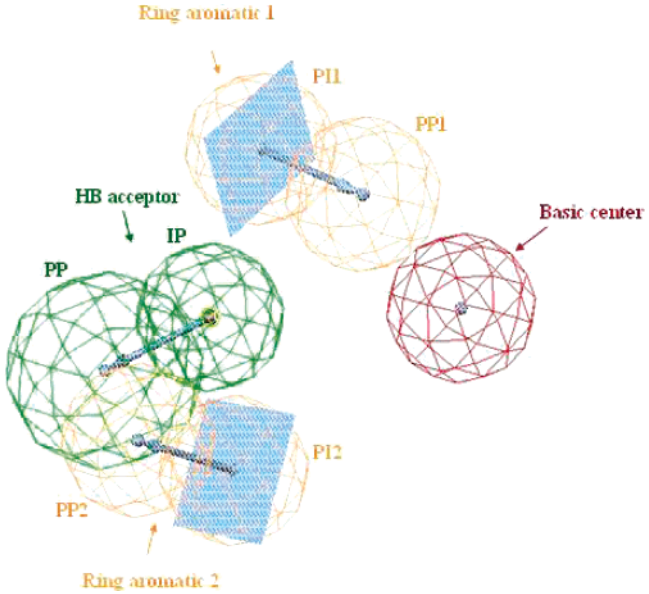

Figure 7. Pharmacophore B.

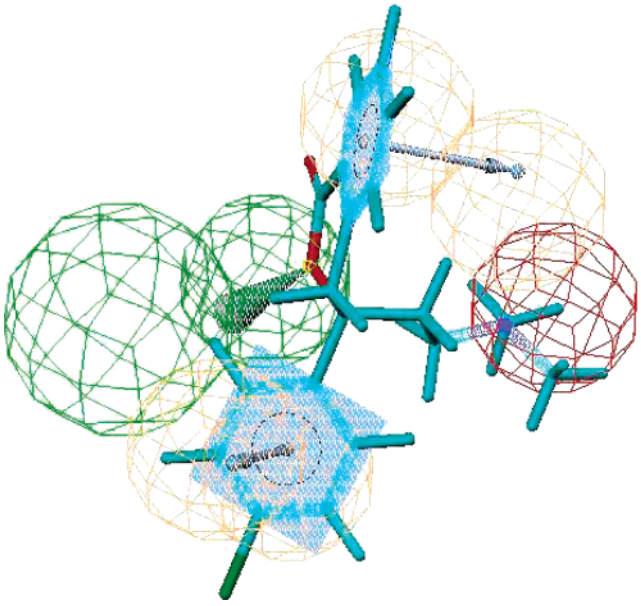

Figure 8. Superimposition between compound **11** and pharmacophore B.

Table 6. Matrix Distances (in Å) for Pharmacophore B

	AR1 (IP1)[a]	AR1 (PP1)	AR2 (IP2)	AR2 (PP2)	basic center	HB acceptor (PP)
AR1 (IP1)						
AR1 (PP1)	2.99					
AR2 (IP2)	7.25	7.21				
AR2 (PP2)	7.07	7.29	2.99			
basic center	5.96	4.72	6.36	8.27		
HB acceptor (PP)	4.56	5.92	3.79	4.69	5.77	
HB acceptor (IP)	7.11	8.79	4.61	5.03	8.54	3.01

[a] AR: aromatic ring. IP: initial point. PP: projected point.

mental three amino acids (Trp7, Lys8, and Tyr9), molecular dynamic simulations were carried out starting from the NMR data. The analysis of the conformational evolution along the trajectory of 500 ps yielded distances of around 6−7 Å for Trp7−Tyr9 (see Figure 10), around 12 Å for Trp7−Lys8 (Figure 11), and around 8−10 Å for Lys8−Tyr9 (Figure 12). The last two values correspond to an evolution toward an

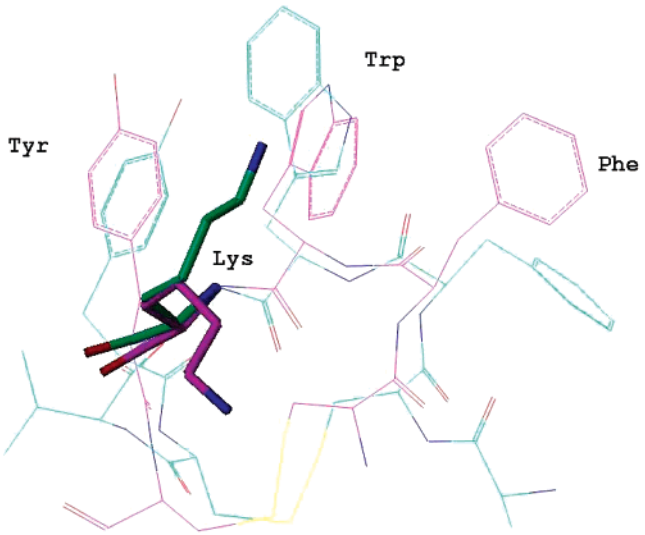

Figure 9. Conformation variation for the Lys8 residue (green for URP and purple for hU-II) between hU-II and URP (NMR data).

Table 7. Matrix Distances (in Å) for the Average Structure of hU-II

	F	W	K	Y
F				
W	8.18			
K	10.06	12.89		
Y	11.08	5.92	10.35	

extended conformation for the Lys residue. The end of this dynamic gave a Trp7−Tyr9 distance in agreement with pharmacophore B for the two simulations URP and hU-II. An average structure of hU-II, along the trajectory, was generated and minimized in an explicit solvent model (Figure 13 and Table 7). This structure showed three β turns of type IV between residues 5−8, 7−10, and 8−11 and an inverse γ turn centered on the sequence Trp−Lys−Tyr ($\phi = -78°$ and $\psi = 32°$ for Lys8). The position of the lysine residue toward the two hydrophobic residues (Trp and Tyr) does not correspond to the distances associated with pharmacophore B. To go further, the conformational flexibility of the lysine residue was analyzed by a systematic search. Of the 343 conformations generated, several could fit pharmacophore B (Trp−Tyr of 7.2 Å, Lys−Tyr of 6.0 Å, and Lys−Trp of 6.4 Å for an optimum fit). These last ones could be favored by π-cation interactions between the amine and the two aromatic rings (Trp and Tyr). The study of Carotenuto et al.[35] from SDS−NMR data of hU-II confirmed these observations with distances close to those of pharmacophore B (Trp−Tyr of 5.8 Å, Lys−Tyr of 6.0 Å, and Lys−Trp of 5.4 Å).

In conclusion, the Trp−Tyr distance around 6−7 Å seems to be constant and independent of the structure (hU-II or URP) or the environment. The distances between the amine and the two hydrophobic groups are more variable. They are around 10 Å in an aqueous medium and around 6 Å in SDS micelles. These last conformations (6 Å) are in agreement with pharmacophore B. At this stage, no conformation of the peptides was found to be close to that of pharmacophore A.

Pharmacophore C toward Nonpeptide Antagonists. Surprisingly, all of the nonpeptide antagonists could fit pharmacophore B with, for some derivatives, more stable

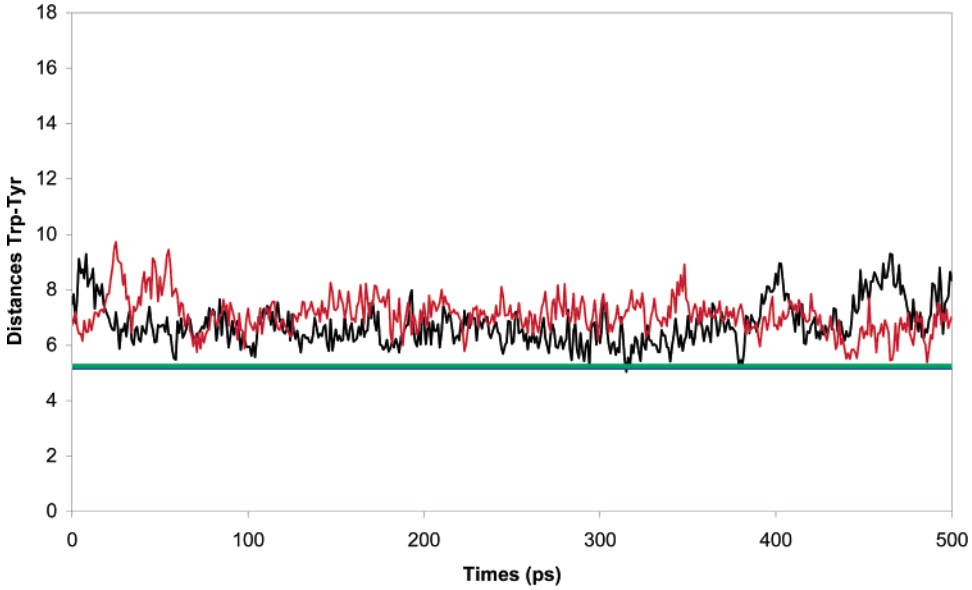

Figure 10. Distances Trp7−Tyr9 (hU-II in black and URP in red) during the production phase. The horizontal lines correspond to the initial distance (NMR data) for URP (green) and hU-II (red).

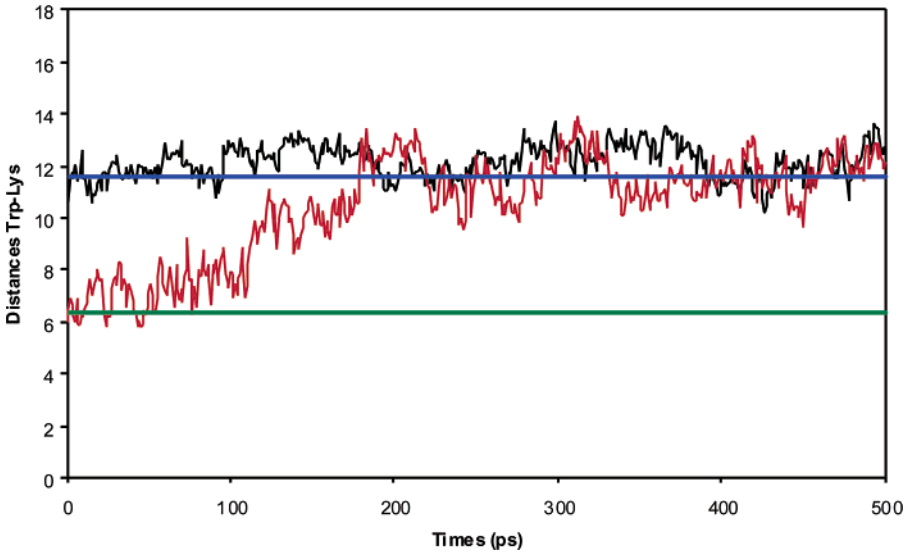

Figure 11. Distances Trp7−Lys8 (hU-II in black and URP in red) during the production phase. The horizontal lines correspond to the initial distance (NMR data) for URP (green) and hU-II (red).

conformations (Table 8). This result shows the difficulty to extract only potential agonists from a database starting from this pharmacophore. But this observation prompted us to explore the possibility of a more complex pharmacophore by a combination of pharmacophores A and B, explaining the affinities of some nonpeptide antagonists but also in agreement with the characteristics of hU-II or URP. Thus, the phenylalanine residue of the peptides was investigated. Starting from the conformation of hU-II which fits pharmacophore B, a Phe−Tyr distance (11 Å) identical to the distance between the two aromatic groups of pharmacophore A (the initial distance Phe−Tyr for hU-II in NMR structure was 9.6 Å) was observed. From this alignment, a third aromatic feature, corresponding to the position of the Phe residue, was added, leading to the pharmacophore called C. This hypothesis was confirmed by fitting hU-II (three hydrophobic groups and one basic center), with the same previous conformation, to pharmacophores A, B, and C, leading in all cases to a very good fit (Figure 14). Moreover, by fitting the nonpeptide antagonists (full fit or partial fit) on pharmacophore C (Table 9), an overall improvement was observed (fit values and stability of the conformations). For the virtual screening based on pharmacophore C, nearly the same molecular scaffolds found in the initial screening appear in this new list. Indeed, this virtual screening (full fit for the compounds selected) leads to 80 compounds instead of 231 compounds, and 86% of these derivatives were present in the initial screening (pharmacophore A). On the six derivatives found as active starting from pharmacophore A for the virtual screening, only **18** and **19** did not fit completely pharmacophore C, but for these derivatives, only one feature is missing.

Previous experiments have demonstrated that the phenylalanine residue is not fundamental for the biological affinities of hU-II or URP.[13,16] Our NMR data showed large different conformations [χ_1 of 183.6° (hU-II) and 60.3° (URP)] for this residue (see Figure 9), and this difference was maintained during the dynamic studies. In agreement with Lavecchia et

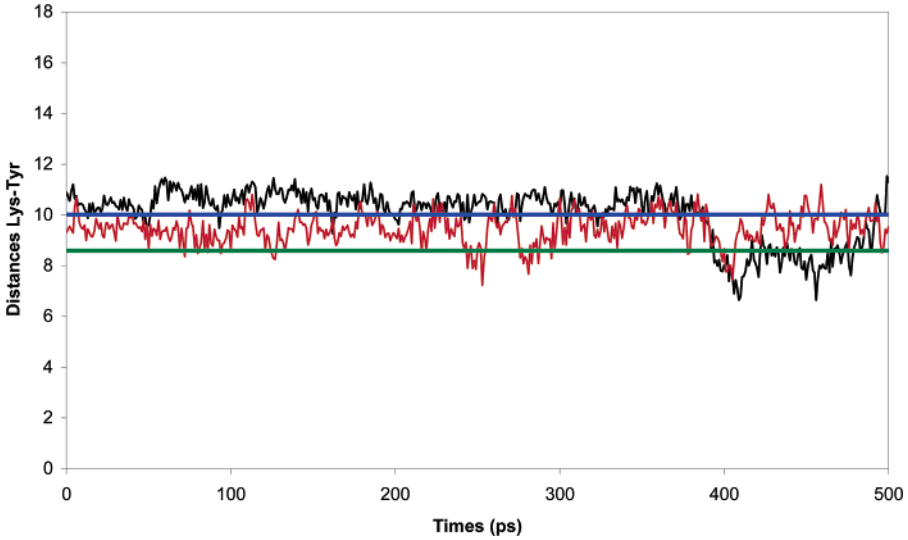

Figure 12. Distances Tyr9−Lys8 (hU-II in black and URP in red) during the production phase. The horizontal lines correspond to the initial distance (NMR data) for URP (green) and hU-II (red).

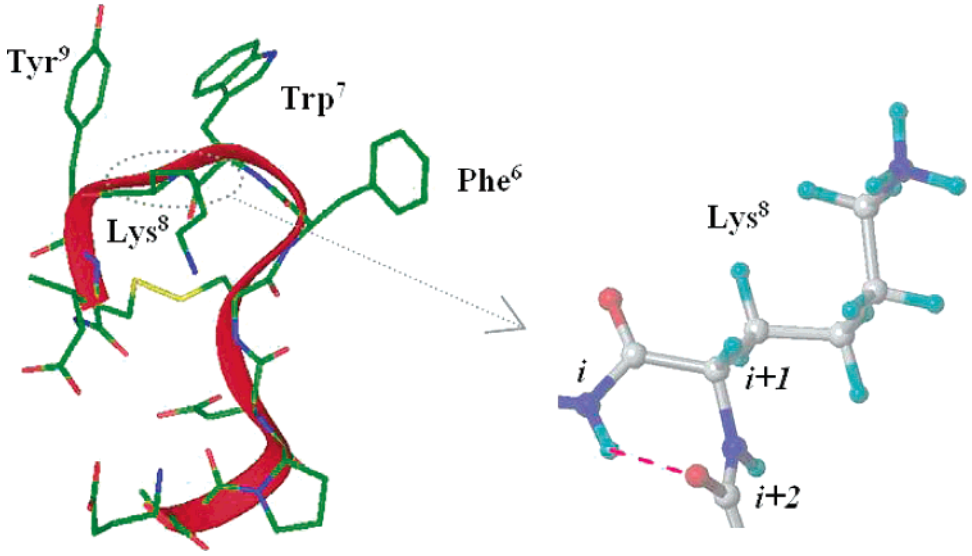

Figure 13. Average structure of hU-II after dynamic study.

Table 8. Pharmacophore A and B Toward Nonpeptide Antagonists

	pharmacophore A		pharmacophore B	
	fit value	relative energy of the conformer (kcal/mol)	fit value	relative energy of the conformer (kcal/mol)
1	3.58	3.53	2.58	11.36
2	2.15	9.37	1.25	9.37
3	2.31	18.15	2.89	13.85
4	3.36	3.04	3.13	8.72
5	0.53	0.65	1.60	4.60
6	0	N/A	1.42	6.09
7	2.03	8.93	2.54	10.23
8	0	N/A	3.12	5.89
9	0	N/A	1.40	4.13
10	2.40	7.25	2.49	1.57

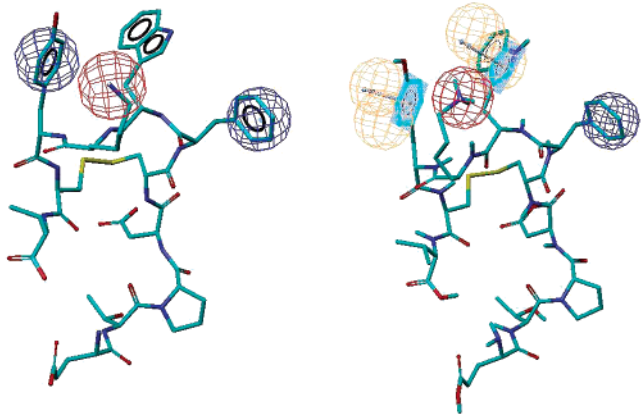

Figure 14. Mapping of structures of hU-II onto pharmacophores A (left) and C (right).

al.[59] concerning the UT-II receptor, a large hydrophobic surface (hydrophobic feature of pharmacophores A and C), situated at the entrance of the transmembrane part, could be considered. The position of this hydrophobic surface could explain the fact that the phenylalanine residue is not fundamental for the biological activity and the phenyl group of this residue could interact with this surface in the two different conformations. A bulky hydrophobic group associated with antagonists like **3**, with two phenyl groups, imitates strongly the two possible positions of the phenylalanine residue (Figure 15). Consequently, the size of the hydrophobic feature present in pharmacophores A and C and

Table 9. Alignment of Nonpeptide Antagonists with Pharmacophore C

	pharmacophore C	
	fit value	relative energy of the conformer (kcal/mol)
1	2.81	2.58
2	2.75	4.67
3	2.55	1.21
4	3.13	8.72
5	1.60	4.60
6	3.11	7.24
7	3.01	4.38
8	2.84	1.61
9	2.05	4.96
10	2.49	1.57
15	2.85	2.53
16	2.79	1.63
17	2.81	9.04
18	2.57	1.02
19	2.91	4.39
20	2.93	2.43

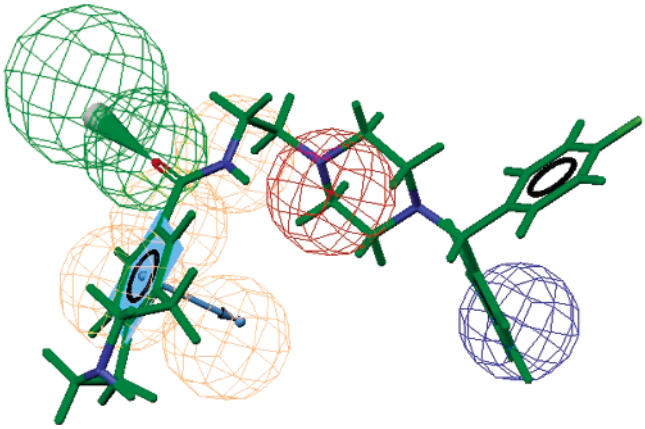

Figure 15. Superimposition between compound **3** and pharmacophore C.

associated with the phenylalanine residue could be defined as a larger domain.

CONCLUSION

We defined, for the first time, pharmacophores for the hU-II antagonists. On the basis of dynamic studies and NMR data, we observed some correlations between the structures of the active peptides (hU-II and URP) and the characteristics of these antagonists. The final proposed model (pharmacophore C) corresponds to the primary sequence FWKY with two aromatic rings, a hydrophobic aromatic group, a hydrogen-bond acceptor, and a basic group. The nonpeptide antagonists or agonists could fit with part of this pharmacophore, i.e., pharmacophores A or B, corresponding to two aromatic−hydrophobic interactions and a polar interaction between the ligands and the receptors. On the basis of pharmacophore A, a virtual screening was carried out, leading to the determination of new families of hU-II antagonists. These compounds appear also as potential hits starting from the more complex pharmacophore C. This result confirms the interest to extract potential ligands from a chemical database.

ACKNOWLEDGMENT

We thank the CRIHAN (Centre de Ressources Informatiques de Haute Normandie) and the European Community (FEDER) for the molecular modeling software. This work was supported by grant from the French Ministry of Research and Technology.

REFERENCES AND NOTES

(1) Pearson, D.; Shively, J. E.; Clark, B. R.; Geschwind, I.; Barkley, M.; Nishioka, R. S.; Bern, H. A. Urotensin II: A somatostatin-like peptide in the caudal neurosecretory system of fishes. *Proc. Natl. Acad. Sci. U.S.A.* **1980**, *77*, 5021−5024.

(2) Coulouarn, Y.; Lihrmann, I.; Jegou, S.; Anouar, Y.; Tostivint, H.; Beauvillain, J. C.; Conlon, J. M.; Bern, H. A.; Vaudry, H. Cloning of the cDNA encoding the urotensin II precursor in frog and human reveals intense expression of the urotensin II gene in motoneurons of the spinal cord. *Proc. Natl. Acad. Sci. U.S.A.* **1998**, *95*, 15803−15808.

(3) Ames, R. S.; Sarau, H. M.; Chambers, J. K.; Willette, R. N.; Aiyar, N. V.; Romanic, A. M.; Louden, C. S.; Foley, J. J.; Sauermelch, C. F.; Coatney, R. W.; Ao, Z.; Disa, J.; Holmes, S. D.; Stadel, J. M.; Martin, J. D.; Liu, W. S.; Glover, G. I.; Wilson, S.; McNulty, D. E.; Ellis, C. E.; Elshourbagy, N. A.; Shabon, U.; Trill, J. J.; Hay, D. W.; Ohlstein, E. H.; Bergsma, D. J.; Douglas, S. A. Human urotensin-II is a potent vasoconstrictor and agonist for the orphan receptor GPR14. *Nature* **1999**, *401*, 282−286.

(4) MacLean, M. R.; Alexander, D.; Stirrat, A.; Gallagher, M.; Douglas, S. A.; Ohlstein, E. H.; Morecroft, I.; Polland, K. Contractile responses to human urotensin-II in rat and human pulmonary arteries: Effect of endothelial factors and chronic hypoxia in the rat. *Br. J. Pharmacol.* **2000**, *130*, 201−204.

(5) Maguire, J. J.; Davenport, A. P. Is urotensin-II the new endothelin? *Br. J. Pharmacol.* **2002**, *137*, 579−588.

(6) Douglas, S. A.; Ohlstein, E. H. Human urotensin-II, the most potent mammalian vasoconstrictor identified to date, as a therapeutic target for the management of cardiovascular disease. *Trends Cardiovasc. Med.* **2000**, *10*, 229−237.

(7) Ong, K. L.; Lam, K. S.; Cheung, B. M. Urotensin II: Its function in health and its role in disease. *Cardiovasc. Drugs Ther.* **2005**, *19*, 65−75.

(8) Matsushita, M.; Shichiri, M.; Imai, T.; Iwashina, M.; Tanaka, H.; Takasu, N.; Hirata, Y. Co-expression of urotensin II and its receptor (GPR14) in human cardiovascular and renal tissues. *J. Hypertens.* **2001**, *19*, 2185−2190.

(9) Totsune, K.; Takahashi, K.; Arihara, Z.; Sone, M.; Ito, S.; Murakami, O. Increased plasma urotensin II levels in patients with diabetes mellitus. *Clin. Sci. (London)* **2003**, *104*, 1−5.

(10) Totsune, K.; Takahashi, K.; Arihara, Z.; Sone, M.; Satoh, F.; Ito, S.; Kimura, Y.; Sasano, H.; Murakami, O. Role of urotensin II in patients on dialysis. *Lancet* **2001**, *358*, 810−811.

(11) Sugo, T.; Murakami, Y.; Shimomura, Y.; Harada, M.; Abe, M.; Ishibashi, Y.; Kitada, C.; Miyajima, N.; Suzuki, N.; Mori, M.; Fujino, M. Identification of urotensin II-related peptide as the urotensin II-immunoreactive molecule in the rat brain. *Biochem. Biophys. Res. Commun.* **2003**, *310*, 860−880.

(12) Bousette, N.; Patel, L.; Douglas, S. A.; Ohlstein, E. H.; Giaid, A. Increased expression of urotensin II and its cognate receptor GPR14 in atherosclerotic lesions of the human aorta. *Atherosclerosis* **2004**, *176*, 117−123.

(13) Flohr, S.; Kurz, M.; Kostenis, E.; Brkovich, A.; Fournier, A.; Klabunde, T. Identification of nonpeptidic urotensin II receptor antagonists by virtual screening based on a pharmacophore model derived from structure-activity relationships and nuclear magnetic resonance studies on urotensin II. *J. Med. Chem.* **2002**, *45*, 1799−1805.

(14) Kinney, W. A.; Almond, H. R., Jr.; Qi, J.; Smith, C. E.; Santulli, R. J.; de Garavilla, L.; Andrade-Gordon, P.; Cho, D. S.; Everson, A. M.; Feinstein, M. A.; Leung, P. A.; Maryanoff, B. E. Structure-function analysis of urotensin II and its use in the construction of a ligand-receptor working model. *Angew. Chem., Int. Ed.* **2002**, *41*, 2940−2944.

(15) Grieco, P.; Carotenuto, A.; Campiglia, P.; Zampelli, E.; Patacchini, R.; Maggi, C. A.; Novellino, E.; Rovero, P. A new, potent urotensin II receptor peptide agonist containing a Pen residue at the disulfide bridge. *J. Med. Chem.* **2002**, *45*, 4391−4394.

(16) Chatenet, D.; Dubessy, C.; Leprince, J.; Boularan, C.; Carlier, L.; Segalas-Milazzo, I.; Guilhaudis, L.; Oulyadi, H.; Davoust, D.; Scalbert, E.; Pfeiffer, B.; Renard, P.; Tonon, M. C.; Lihrmann, I.; Pacaud, P.; Vaudry, H. Structure−activity relationships and structural conformation of a novel urotensin II-related peptide. *Peptide* **2004**, *25*, 1819−1830.

(17) Aissaoui, H.; Binkert, C.; Clozel, M.; Mathys, B.; Mueller, C.; Nayler, O.; Scherz, M.; Velker, J.; Weller, T. Preparation of 1-(piperazinylalkyl)-3-quinolinylurea derivatives as urotensin II antagonists. *PCT Int. Appl*. **2004**, *WO 2004099179*, 63.
(18) Aissaoui, H.; Binkert, C.; Clozel, M.; Mathys, B.; Mueller, C.; Nayler, O.; Scherz, M.; Verker, J.; Weller, T. Preparation of novel piperidine derivatives as urotensin II antagonists. *PCT Int. Appl*. **2004**, *WO 2004099180*, 32.
(19) Aissaoui, H.; Binkert, C.; Clozel, M.; Mathys, B.; Mueller, C.; Nayler, O.; Scherz, M.; Weller, T. Preparation of 1,2,3,4-tetrahydroisoquinolinyl ureas and related derivatives as urotensin II receptor antagonists. *PCT Int. Appl*. **2002**, *WO 2002076979*, 94.
(20) Mathys, B.; Mueller, C.; Scherz, M.; Weller, T.; Clozel, M.; Velker, J.; Bur, D. Preparation of pyridinyl ureas as urotensin II antagonists. *PCT Int. Appl*. **2005**, *WO2005030209*, 113.
(21) Kikkawa, H.; Kushida, H. Sulfonamides, and pharmaceutical compositions containing them, for the treatment of inflammatory bowel diseases. *PCT Int. Appl*. **2005**, *WO2005072226*, 19.
(22) Clozel, M.; Binkert, C.; Birker-Robaczewska, M.; Boukhadra, C.; Ding, S. S.; Fischli, W.; Hess, P.; Mathys, B.; Morrison, K.; Muller, C.; Muller, C.; Nayler, O.; Qiu, C.; Rey, M.; Scherz, M. W.; Velker, J.; Weller, T.; Xi, J. F.; Ziltener, P. Pharmacology of the urotensin-II receptor antagonist palosuran (ACT-058362; 1-[2-(4-benzyl-4-hydroxypiperidin-1-yl)-ethyl]-3-(2-methyl-quinolin-4-yl)-urea sulfate salt): First demonstration of a pathophysiological role of the urotensin system. *J. Pharmacol. Exp. Ther*. **2004**, *311*, 204−212.
(23) Tarui, N.; Santo, T.; Watanabe, H.; Aso, K.; Ishihara, Y. Preparation of 2,3,4,5-tetrahydro-1H-3-benzazepine derivatives as GPR14 antagonists. *PCT Int. Appl*. **2002**, *WO 2002002530*, 217.
(24) Tarui, N.; Santo, T.; Watanabe, H.; Aso, K.; Miwa, T.; Takekawa, S. Preparation of biphenylcarboxamide compounds as GPR14 antagonists or somatostatin receptor regulators. *PCT Int. Appl*. **2002**, *WO 2002000606*, 274.
(25) Tarui, N.; Santo, T.; Mori, M.; Watanabe, H. Quinoline derivatives as vasoactive agents exhibiting orphan receptor GPR14 protein antagonism. *PCT Int. Appl.* **2001**, *WO 2001066143*, 97.
(26) Jin, J.; Dhanak, D.; Knight, S. D.; Widdowson, K.; Aiyar, N.; Naselsky, D.; Sarau, H. M.; Foley, J. J.; Schmidt, D. B.; Bennett, C. D.; Wang, B.; Warren, G. L.; Moore, M. L.; Keenan, R. M.; Rivero, R. A.; Douglas, S. A. Aminoalkoxybenzyl pyrrolidines as novel human urotensin-II receptor antagonists. *Bioorg. Med. Chem. Lett.* **2005**, *15*, 3229−3232.
(27) Dhanak, D.; Knight, S. D. Sulfonamide derivative urotensin-II receptor antagonists, preparation, pharmaceutical compositions, and therapeutic use. *PCT Int. Appl.* **2001**, *WO2001045694*, 40.
(28) Dodson, J. W.; Ghavimi-Alagha, B.; Girard, G. R.; King, B. W.; McAtee, J. J.; Neeb, M. J.; Wang, N.; Yuan, C. C. K. Preparation of sulfonamides as antagonists of urotensin II. *PCT Int. Appl.* **2004**, *WO2004043366*, 82.
(29) Barton, L. S.; Dodson, J. W.; Gaitanopoulos, D. E.; Girard, G. R.; King, B. W.; McAtee, J. J.; Neeb, M. J. Preparation of sulfonamides as antagonists of urotensin II. *PCT Int. Appl*. **2004**, *WO2004043917*, 81.
(30) Dhanak, D.; Gallagher, T. F.; Knight, S. D.; Schmidt, S. J. Preparation of sulfonamides as antagonists of urotensin II. *PCT Int. Appl*. **2002**, *WO2002089785*, 35.
(31) Dhanak, D.; Knight, S. D.; Jin, J.; Rivero, R. A. Preparation of pyrrolidine sulfonamides as urotensin II antagonists. *PCT Int. Appl*. **2002**, *WO2002078641*, 19.
(32) Dhanak, D.; Knight, S. D. Preparation of quinolones as urotensin-II receptor antagonists. *PCT Int. Appl.* **2002**, *WO2002047456*, 16.
(33) Croston, G. E.; Olsson, R.; Currier, E. A.; Burstein, E. S.; Weiner, D.; Nash, N.; Severance, D.; Allenmark, S. G.; Thunberg, L.; Ma, J. N.; Mohell, N.; O'Dowd, B.; Brann, M. R.; Hacksell, U. Discovery of the first nonpeptide agonist of the GPR14/urotensin-II receptor: 3-(4-chlorophenyl)-3-(2-(dimethylamino)ethyl) isochroman-1-one (AC-7954). *J. Med. Chem.* **2002**, *45*, 4950−4953.
(34) Olsson, R. A combinatorial scaffold approach towards the pharmacophores of ligands to urotensin II and somatostatin 5 receptors. *PCT Int Appl*. **2004**, *WO 2004073642*, 29.
(35) Carotenuto, A.; Grieco, P.; Campiglia, P.; Novellino, E.; Rovero, P. Unraveling the active conformation of urotensin II. *J. Med. Chem.* **2004**, *47*, 1652−1661.
(36) Brooks, B. R.; Bruccoleri, R. E.; Olafson, B. D.; Sates, D. J.; Swaninathan, S.; Karplus, M. CHARMM: A program for macromolecular energy, minimization, and dynamics calculations. *J. Comput. Chem.* **1983**, *4*, 187−217.
(37) Smellie, A.; Teig, S. L.; Towin, P. Poling: Promoting conformational variation. *J. Comput. Chem.* **1995**, *16*, 171−187.
(38) States, D. J.; Haberkorn, R. A.; Ruben, D. J. A two-dimensional nuclear Overhauser effect experiment with pure absorption phase in four quadrants. *J. Magn. Reson.* **1982**, *48*, 286−292.
(39) Sklenar, V.; Piotto, M.; Leppik, R.; Saudek, V. Gradient-tailored water suppression for 1H-15N HSQC experiments optimized to retain full sensitivity. *J. Magn. Reson.* **1933**, *102*, 241−245.
(40) Aue, W. P.; Bartholdi, E.; Ernst, R. R. Two-dimensional spectroscopy. Application to Nuclear Magnetic Resonance. *J. Chem. Phys*. **1976**, *64*, 2229−2246.
(41) Braunschweiler, L.; Ernst, R. R. Coherence transfer by isotropic mixing: Application to proton correlation spectroscopy. *J. Magn. Reson.* **1983**, *53*, 521−528.
(42) Jeener, J.; Meier, B. H.; Bachmann, P.; Ernst, R. R. Investigation of exchange process by two-dimensional NMR spectroscopy. *J. Chem. Phys.* **1979**, *71*, 4546−4553.
(43) Kumar, A.; Ernst, R. R.; Wuthrich, K. A two-dimensional nuclear Overhauser enhancement (2D NOE) experiment for the elucidation of complete proton−proton cross-relaxation networks in biological macromolecules. *Biochem. Biophys. Res. Commun.* **1980**, *95*, 1−6.
(44) Pardi, A.; Billeter, M.; Wüthrich, K. Calibration of the angular dependence of the amide proton-C^{α} proton coupling constants, $^{3}JHN_{\alpha}$, in a globular protein: Use of $^{3}JHN_{\alpha}$ for identification of helical secondary structure. *J. Mol. Biol.* **1984**, *180*, 741−751.
(45) Nilges, M.; Gronenborn, A. M.; Brunger, A. T.; Clore, G. M. Determination of three-dimensional structures of proteins by simulated annealing with interproton distance restraints. Application to crambin, potato carboxypeptidase inhibitor and barley serine proteinase inhibitor 2. *Protein Eng*. **1988**, *2*, 27−38.
(46) MacKerell, J. A. D.; Bashford, D.; Bellott, M.; Dunbrack, J. R. L.; Evanseck, J. D.; Field, M. J.; Fischer, S.; Gao, J.; Guo, H.; Ha, S.; Joseph-McCarthy, D.; Kuchnir, L.; Kuczera, K.; Lau, F. T. K.; Mattos, C.; Michnick, S.; Ngo, T.; Nguyen, D. T.; Prodhom, B.; Reiher, I. W. E.; Roux, B.; Schlenkrich, M.; Smith, J. C.; Stote, R.; Straub, J.; Watanabe, M.; Wiorkiewicz-Kuczera, J.; Yin, D.; Karplus, M. All-atom empirical potential for molecular modeling and dynamics studies of proteins. *J. Phys. Chem. B* **1988**, *102*, 3586−3616.
(47) Jorgensen, W. L.; Chandrashekar, J.; Madura, J. D.; Impey, R.; Klein, M. L. Refined TIP3P model for water. *J. Chem. Phys.* **1983**, *79*, 926−935.
(48) Dubs, A.; Wagner, G.; Wuthrich, K. Individual assignments of amide proton resonances in the proton NMR spectrum of the basic pancreatic trypsin inhibitor. *Biochim. Biophys. Acta* **1979**, *577*, 177−194.
(49) Wagner, G.; Kumar, A.; Wuthrich, K. Systematic application of two-dimensional ^{1}H nuclear-magnetic-resonance techniques for studies of proteins. *Eur. J. Biochem.* **1981**, *114*, 375−384.
(50) Wüthrich, K.; Billeter, M.; Braun, W. Polypeptide secondary structure determination by nuclear magnetic resonance observation of short proton−proton distances. *J. Mol. Biol.* **1984**, *180*, 715−740.
(51) Wüthrich, K., In *NMR of Proteins and Nucleic Acids*; Wiley: New York, 1986.
(52) Wagner, G.; Wüthrich, K. Sequential resonance assignments in protein ^{1}H nuclear magnetic resonance spectra: Basic pancreatic trypsin inhibitor. *J. Mol. Biol.* **1982**, *155*, 347−366.
(53) Englander, S. W.; Kallenbach, N. R. Hydrogen exchange and structural dynamics of proteins and nucleic acids. *Q. Rev. Biophys.* **1984**, *16*, 521−665.
(54) Wagner, G.; Wüthrich, K. Amide protein exchange and surface conformation of the basic pancreatic trypsin inhibitor in solution. Studies with two-dimensional nuclear magnetic resonance. *J. Mol. Biol*. **1982**, *160*, 343−361.
(55) Redfield, C.; Dobson, C. M. Sequential ^{1}H NMR assignments and secondary structure of hen egg white lysozyme in solution. *Biochemistry* **1988**, *27*, 122−136.
(56) Wagner, G. Characterization of the distribution of internal motions in the basic pancreatic trypsin inhibitor using a large number of internal NMR probes. *Q. Rev. Biophys.* **1983**, *16*, 1−57.
(57) Wüthrich, K.; Wider, G.; Wagner, G.; Braun, W. Sequential resonance assignments as a basis for determination of spatial protein structures by high resolution proton nuclear magnetic resonance. *J. Mol. Biol.* **1982**, *155*, 311−319.
(58) Csizmadia, F. JChem: Java applets and modules supporting chemical database handling from web browsers. *J. Chem. Inf. Comput. Sci.* **2000**, *40*, 323−324.
(59) Lavecchia, A.; Cosconati, S.; Novellino, E. Architecture of the human urotensin II receptor: Comparison of the binding domains of peptide and non-peptide urotensin II agonists. *J. Med. Chem.* **2005**, *48*, 2480−2492.

CI6003948